IEEE Photonics Journal
An IEEE Photonics Society Publication

Multiple Fano Resonances Based on Plasmonic Resonator System With End-Coupled Cavities for High-Performance Nanosensor

Volume 9, Number 6, December 2017

Chao Li
Shilei Li
Yilin Wang
Rongzhen Jiao
Lulu Wang
Li Yu

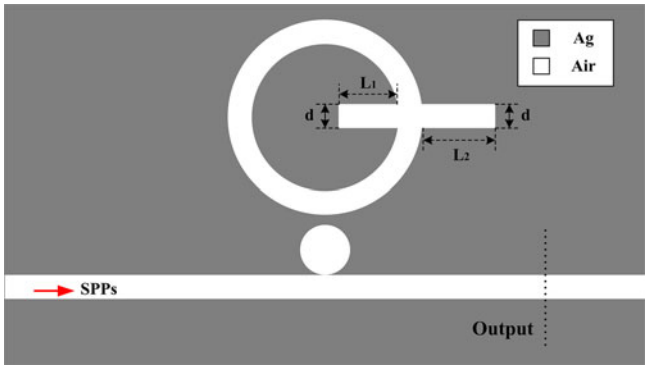

DOI: 10.1109/JPHOT.2017.2763781
1943-0655 © 2017 IEEE

IEEE photonics SOCIETY
IEEE

Multiple Fano Resonances Based on Plasmonic Resonator System With End-Coupled Cavities for High-Performance Nanosensor

Chao Li,[1,2] **Shilei Li**,[1,2] **Yilin Wang**,[1,2] **Rongzhen Jiao**,[1,2] **Lulu Wang**,[1,2] **and Li Yu** [1,2]

[1]State Key Laboratory of Information Photonics and Optical Communications, Beijing University of Posts and Telecommunications, Beijing 100876 China
[2]School of Science, Beijing University of Posts and Telecommunications, Beijing 100876 China

DOI:10.1109/JPHOT.2017.2763781

Manuscript received August 2, 2017; revised September 26, 2017; accepted October 12, 2017. Date of publication October 19, 2017; date of current version October 31, 2017. This work was supported in part by the National Natural Science Foundation of China under Grants 11574035, 11374041, 61571060, and 11404030, and in part by the Fund of State Key Laboratory of Information Photonics and Optical Communications, Beijing University of Posts and Telecommunications, PR China. Corresponding author: Li Yu (e-mail: yuliyuli@bupt.edu.cn).

Abstract: A plasmonic resonator system composed of a metal-insulator-metal waveguide coupled with a disk and a ring cavity was proposed to produce double Fano resonances, which resulted from the coupling between the narrow discrete resonances of the ring cavity and the broad spectrum of the disk resonator. Based on the proposed structure, end-coupled cavities are added to form new coupled plasmonic resonator systems, which can support triple and quadruple Fano resonances, and the multiple Fano resonances can be tuned semi-independently by changing the parameters of the end-coupled cavities. These characteristics offer flexibility in the design of the highly integrated circuits. Also, the proposed structure can work as a highly efficient plasmonic nanosensor, which yields a sensitivity of $\sim$1100 nm/RIU and figure of merit (FOM) of $\sim 2.73 \times 10^4$. The proposed structure may have potential applications for nanosensing, slow light, and nonlinear devices in highly integrated devices.

Index Terms: Surface plasmons, fano resonance, plasmonic waveguide, sensor.

1. Introduction

Fano resonance is the coupling effect which results from the coherent interference between a discrete state and a continuous state [1]. Because of the sharp asymmetric spectral line-shape and the strong field enhancement, Fano resonances have a broad range of applications in sensors, modulators, slow light and nonlinear processes [2]–[5]. In recent years, Fano resonances in metallic nanostructure have attracted enormous attention, since surface plasmon polaritons (SPPs) can overcome the diffraction limit and confine light in deep sub-wavelength dimensions [6]. A variety of plasmonic structures have been proposed to realize the Fano resonance, such as ring or disk cavities [7]–[9], plasmonic nanoclusters [10]–[12], optical antennas [13]–[15], nano-slits [3], [16], and metal-insulator-metal (MIM) waveguide structures [17]–[21]. Among all the structures, the MIM

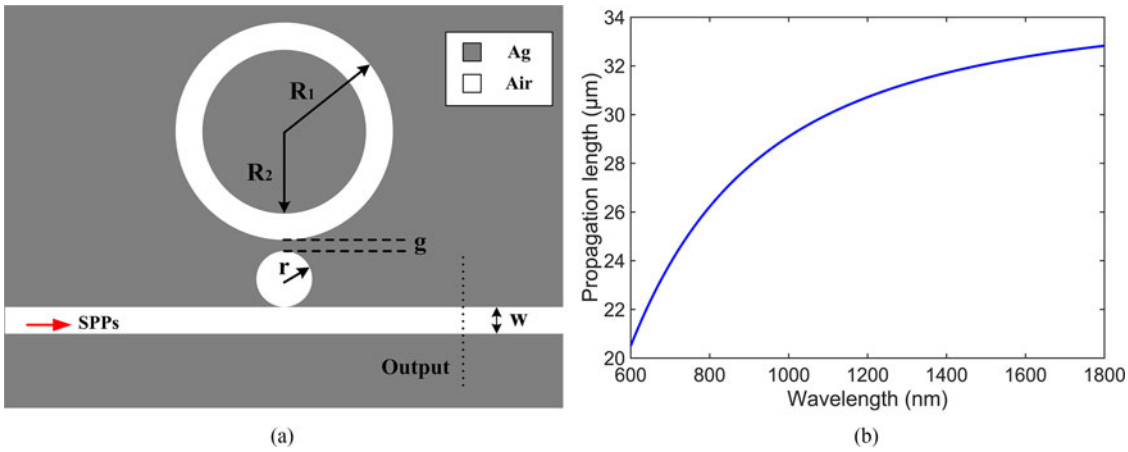

Fig. 1. (a) Schematic for the plasmonic resonator system composed of a MIM waveguide coupled with a disk and a ring cavity. (b) The propagation length of the proposed structure.

waveguide structures have gained more attention because these structures are more suitable for the highly integrated photonic circuits due to their deep sub-wavelength confinement of light. And based on the MIM waveguides, a large number of devices, such as splitters [22], [23], filters [24], [25], sensors [2], [17], [26], and slow-light devices [27], [28] have been designed and demonstrated in theory and experiment. Recently, the multiple Fano resonances become more important and have gained much attention due to the advantage for enhanced bio-chemical sensing, multicolor spectroscopy and broadband nonlinear processes [29]–[31]. Moreover, it is desirable to actively tune the Fano resonances in practical applications for optical computing and processing. However, because the multiple Fano resonances are caused by the collective behavior of the total plasmonic systems, it is difficult to make an independent and precise tuning for the multiple Fano resonances.

In this paper, tunable multiple Fano resonances are realized in coupled plasmonic resonator system. Firstly, a plasmonic resonator system composed of a MIM waveguide coupled with a disk and a ring cavity is investigated. The double Fano resonances produced by this structure originate from the coupling between the narrow discrete resonances of the ring cavity and the broad spectrum of the disk resonator. Based on the proposed structure, a stub cavity and a groove cavity are added in succession, so as to form new coupled plasmonic resonator systems which can support triple and quadruple Fano resonances. Because the multiple Fano resonances originate from different mechanisms, they can be tuned semi-independently by changing the parameters of the stub or groove cavity. Simulation results also show that the proposed structure can work as a highly efficient plasmonic nanosensor with a sensitivity of $\sim$1100 nm/RIU and figure of merit (FOM) of $\sim 2.73 \times 10^4$. The proposed structure may provide a new way to realize independently tunable multiple Fano resonances and may have potential applications for sensing, slow light and nonlinear devices in highly integrated devices.

2. Structure Model and Theoretical Analysis

The basic scheme of the plasmonic resonator system is shown in Fig. 1, which is composed of a MIM waveguide coupled with a disk and a ring cavity. The system is a two-dimensional model, the gray and white parts are defined as Ag and Air, respectively. The total length of the structure is 3 μm. The width of the MIM waveguide is set as w $=$ 50 nm to cut off higher-order modes. The radius of the disk is r $=$ 50 nm, the outer and inner radii of the ring resonator are $R_1 = 250$ nm and $R_2 = 200$ nm, respectively. This set the resonance wavelength of our system in the range of visible and near infrared, which is very useful to photonic applications. The coupling distance between the disk and ring cavity is g $=$ 10 nm, which is limited by the nanofabrication techniques. In order to investigate the optical properties of the proposed system, the transmission spectra are

numerically calculated using the finite-difference time-domain (FDTD) method. PML layers are set at the boundaries of the structure, and the grid size is set as 4 nm $\times$ 4 nm. In order to excite SPPs, the input light is set to be transverse magnetic (TM) mode source. The optical constants of Ag are obtained from the experiment data by Johnson and Christy [32].

In practical applications, ohmic losses of plasmonic waveguides have great influence on the SPPs transmission, so the size of structures must be paid attention to. The effective length of such structures is mainly determined by the propagation length of SPP which is defined as $L_{spps} = \lambda_0/[4\pi \mathrm{Im}(n_{eff})]$, where λ_0 is the free-space photon wavelength and n_{eff} is the effective refractive index of the waveguide. The calculated propagation length is shown in Fig. 1(b). The result shows that the propagation length is longer than 20 μm in the range of visible and near infrared, which is much larger than the size of the proposed structure so the ohmic losses can be ignored.

For a MIM waveguide coupling resonator, the resonance wavelength can be determined by the standing wave theory [25], [33]:

$$\lambda = \frac{2n_{eff}L_{eff}}{N - \varphi/\pi} \tag{1}$$

Where n_{eff} represents the effective index of the SPPs in the MIM waveguide which can be obtained by solving the eigenfunction of the MIM waveguide, φ is the phase shift introduced by the SPP reflection off the metal wall in the resonator, L_{eff} represents the effective length of the resonator and N represents the resonance orders in the cavity. Based on (1), it can be obtained that the dependence of the variation of the resonant wavelength on the resonator length L_{eff} is:

$$\frac{d\lambda}{dL_{eff}} = \frac{2n_{eff}}{N - \varphi/\pi} \tag{2}$$

The transmission spectrum of the disk-ring resonator system in Fig. 1(a) is displayed in Fig. 2(a). The calculated transmission spectrum contains double Fano resonances called as FR_1 and FR_2, respectively. The transmission spectra of the disk and single ring cavity are also calculated. The disk represents a broad transmission spectrum with a dip at $\lambda = 884$ nm, while the transmission spectrum of the single ring cavity contains two narrow and discrete dips at $\lambda = 678$ nm and $\lambda = 995$ nm, respectively. The origin of the two sharp Fano resonances FR_1 and FR_2 can be explained by the interference of the narrow discrete state (ring cavity) and the broad continuum state (disk). The coherence properties (constructive or destructive) are reverse near the opposite sides of the resonant wavelength, forming the asymmetric Fano resonance line-shapes. To further understand the underlying physics of the Fano resonances in the proposed system, the distribution of normalized magnetic field intensity ($|H_z|^2$) at the peak of FR_1 ($\lambda = 685$ nm) and FR_2 ($\lambda = 996$ nm) are displayed in Fig. 2(b) and (c), respectively. It can be seen that almost all the energy confined in the ring cavity at FR_1 and FR_2, indicating that both FR_1 and FR_2 are influenced by the ring cavity. FR_1 and FR_2 can be distinguished by the resonant orders of the ring cavity which indicate that FR_1 represents the $N = 6$ order ring mode and FR_2 represents the $N = 4$ order ring mode. The effective length of the ring cavity can be approximated as $L_{eff} = 2 \times \pi \times (R_1 + R_2)/2$, and it can be calculated that the effective refractive index of the SPPs in this MIM waveguide is $n_{eff} = 1.46$ at $\lambda = 685$ nm and $n_{eff} = 1.41$ at $\lambda = 996$ nm, so based on (1), it is easy to obtain that the resonant wavelength of FR_1 and FR_2 are $\lambda = 688$ nm and $\lambda = 997$ nm, which corresponds well with the simulation results.

As the Fano resonance is induced by the coupling between the disk and ring resonator, the transmittance and wavelength of the Fano peaks will be affected by the gap size g. Moreover, since the accuracy of fabrication must be considered in the realization of the device, it is vital to investigate the fabrication tolerances for the proposed structure. We calculated the transmission spectra of the disk-ring resonator system for different gap size g from 10 nm to 18 nm, which are shown in Fig. 2(d). The result shows that while the transmittance of the Fano peaks decrease with increasing gap size, the wavelength of the Fano peaks have little change, which indicates good stability of the characteristics of the structure.

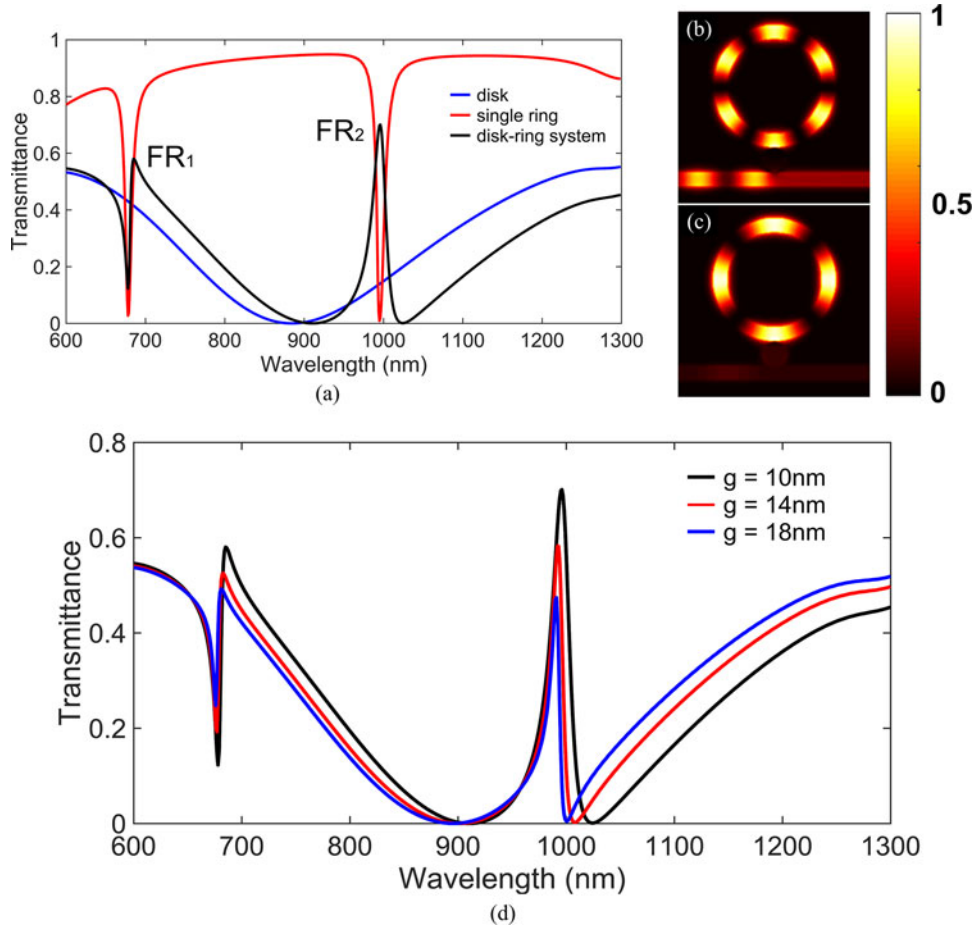

Fig. 2. (a) Transmission spectra of the plasmonic resonator system: The blue, red and black curves represent the transmission spectrum of the disk resonator, the single ring cavity and the disk-ring resonator system, respectively. The parameters are set as w = 50 nm, r = 50 nm, R_1 = 250 nm, R_2 = 200 nm and g = 10 nm. (b) and (c) The distribution of normalized magnetic field intensity ($|H_z|^2$) at λ = 685 nm and λ = 996 nm, respectively. (d) Transmission spectra of the plasmonic resonator system with different coupling gap sizes.

3. Transmission Properties of the Extended Structure

The disk-ring resonator system discussed above is flexible and can be easily extended to a multiple Fano resonances system by adding derivative structures.

3.1 Triple Fano Resonances Induced by Adding an End-Coupled Stub Cavity

Herein, an end-coupled stub cavity is added to the right side of the inner disk of the ring cavity, as shown in Fig. 3(a). In order to investigate the optical properties of the proposed structure, the transmission spectrum is numerically calculated, as shown in Fig. 3(b). The width and length of the stub cavity are set as d = 50 nm and L_1 = 100 nm, respectively. Comparing to the transmittance spectrum of the disk-ring resonator system, it can be seen that FR_1 is slightly moved, while FR_2 vanishes and double new Fano resonance line-shapes arise. We call them new Fano resonance 1 (NFR_1) and new Fano resonance 2 (NFR_2), for the convenience of discussion. To explain the origin of the triple Fano resonance in this stub-coupled system, the distribution of normalized magnetic field intensity ($|H_z|^2$) at the peak of FR_1 (λ = 681 nm), NFR_1 (λ = 772 nm) and NFR_2 (λ = 1085 nm) are numerically calculated as displayed in Fig. 3(c)–(e), respectively. The field distribution at FR_1 is almost exactly the same with which shown in Fig. 2(b), indicating that it is still the ring mode and is

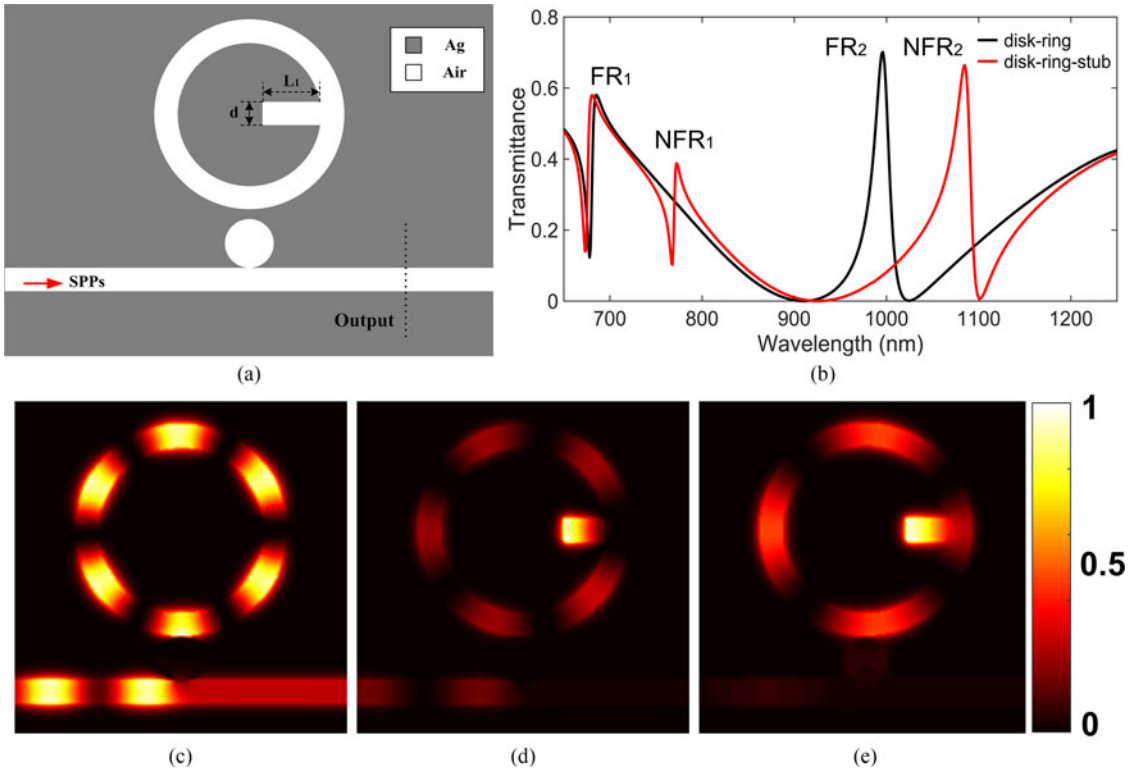

Fig. 3. (a) Schematic for the disk-ring resonator system added with an end-coupled stub cavity. (b) Transmission spectra of the plasmonic resonator system: the black and red curves represent the transmission spectrum of the disk-ring system and disk-ring-stub system, respectively. The parameters are set as d = 50 nm and L_1 = 100 nm. (c)–(e) The distribution of normalized magnetic field intensity ($|H_z|^2$) at λ = 681 nm, λ = 772 nm and λ = 1085 nm, respectively.

not affected by the stub cavity. It is noticed that the stub cavity is located at the node of the 3rd ring mode, so it will not be coupled to this mode. While the field distributions at NFR_1 and NFR_2 are of a big difference where the magnetic field intensity are confined in the stub cavity, indicating that the stub cavity is coupled to the ring cavity and generate two new modes which can be called as the stub modes.

Furthermore, it is found that the transmission spectrum of the proposed structure can be tuned by changing the parameters of its components. Herein, we calculated the tuning of the resonant wavelengths on the variable L_1 and the other parameters keep fixed. When L_1 alters from 80 nm to 120 nm, the transmission spectra are displayed in Fig. 4(a)–(e), respectively. It can be seen that FR_1 keeps fixed through changing the length of the stub cavity, which confirms that FR_1 is the ring mode so it will not be affected by changing the length of the stub cavity. NFR_1 and NFR_2 both make a red shift with the length of stub cavity increasing from 80 nm to 120 nm, as NFR_1 from 743 nm to 803 nm and NFR_2 from 1060 nm to 1114 nm, respectively. According to (2), the resonant wavelength is proportional to the effective length of the cavity, which can lead to the result that $\Delta\lambda \propto \Delta L_1$. This implies linear red shift in the resonant wavelength and is consistent with the symbol lines in Fig. 4.

Successively, we investigate the sensing performance of our structure. Sensing is one of the most important applications of Fano resonance. The sensitivity (S) and the figure of merit (FOM) are two key parameters widely used to evaluate the sensing performance of the Fano resonance, as expressed as $S = d\lambda/dn(\lambda)$ and $FOM = \Delta T/T\Delta n$ [18], [34], where $\Delta T/\Delta n$ represents the transmittance variation induced by the change of refractive index. It can be predicted that an ultra-low transmittance and a sharp increase of the transmittance induced by refractive index changes

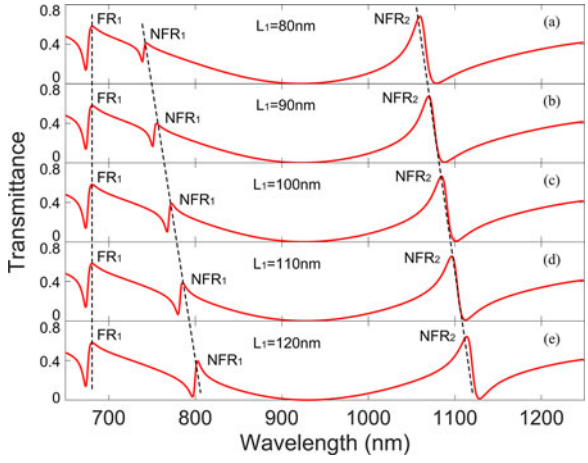

Fig. 4. (a)–(e) Transmission spectra for variable L_1 with d = 50 nm.

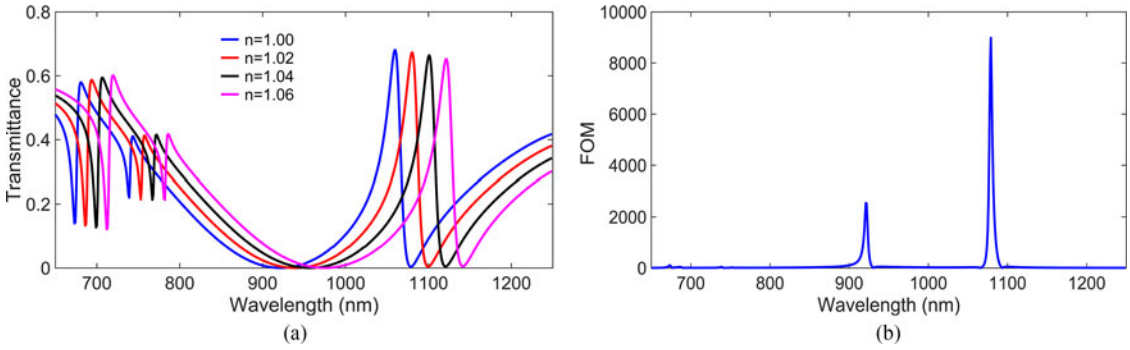

Fig. 5. (a) Transmission spectra for different refractive index. (b) The calculated FOM at different wavelength, the parameters are set as $L_1 = 80$ nm, d = 50 nm.

are preferred for obtaining a high FOM. We calculated the sensing performance of the proposed structure, and the results are shown in Fig. 5(a) and (b). The resonant wavelength has a red shift with refractive index increasing from 1 to 1.06. The proposed structure has a good sensitivity, about 650 nm/RIU for FR_1, 750 nm/RIU for NFR_1 and 1000 nm/RIU for NFR_2, which is better compared with those in the references [2], [21], [35]. The FOM curve is shown in Fig. 5(b), and the maximum can reach as FOM = 8984 at $\lambda = 1079$ nm, which is higher than those plasmonic sensors reported previously [17], [18], [26]. The outstanding sensing performance is due to ultra-sharp Fano line shapes, which results in sharp change of transmittance induced by refractive index variations.

3.2 Quadruple Fano Resonances Induced by Adding Another Groove Cavity

To further investigate the multiple Fano resonances in this system, another groove cavity is added to the right side of the outer disk of the ring cavity, as shown in Fig. 6(a). The width of the stub cavity and groove cavity are fixed as d = 50 nm, and the length of the stub cavity and groove cavity are set as $L_1 = 100$ nm and $L_2 = 160$ nm, respectively. The transmission spectrum of the proposed structure is shown in Fig. 6(b), and the transmission spectra of structures which contains single stub or groove cavity are also calculated. The calculated transmission spectrum contains quadruple Fano resonances, and two more new Fano resonance line-shapes emerge which are called as new Fano resonance 3 (NFR_3) and new Fano resonance 4 (NFR_4). It is noticed that the transmission spectrum of the proposed structure coincides with single stub-coupled structure at FR_1 and NFR_1, indicating that FR_1 still represents the ring mode and NFR_1 still represents the stub mode according to the discussion in Section 3.1. Meanwhile, it coincides with single groove-coupled structure at

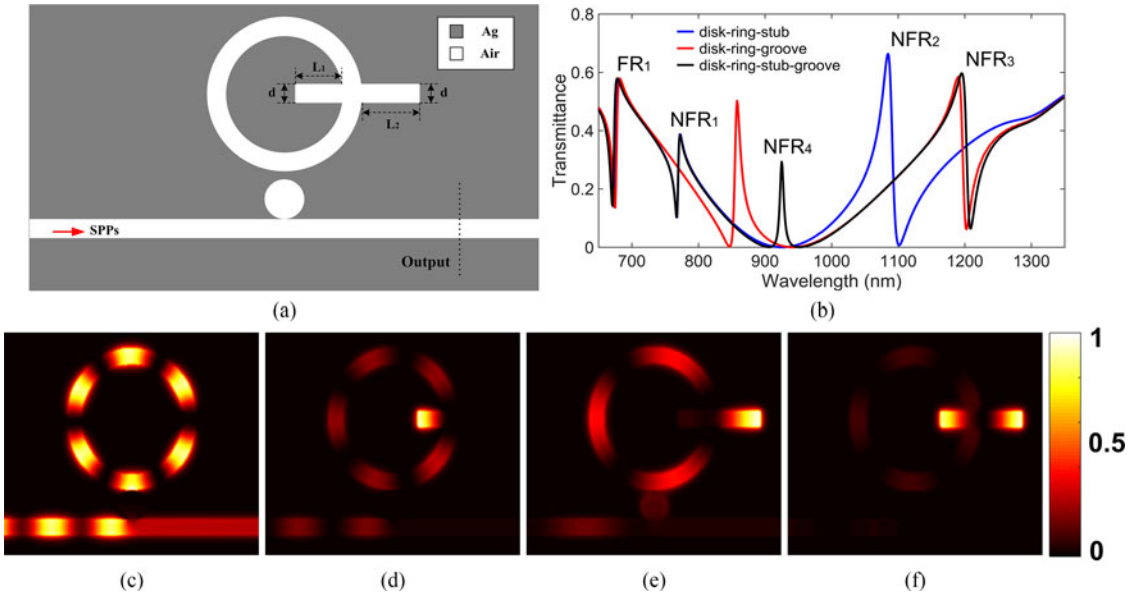

Fig. 6. (a) Schematic for the disk-ring-stub resonator system added with another groove cavity. (b) Transmission spectra of the plasmonic resonator system: the blue and red curves represent the transmission spectrum of the disk-ring-stub system and disk-ring-groove system, respectively. The black curve represents the transmission spectrum of the disk-ring-stub-groove system. The parameters are set as $d = 50$ nm, $L_1 = 100$ nm and $L_2 = 160$ nm. (c)–(f) The distribution of normalized magnetic field intensity ($|H_z|^2$) at $\lambda = 678$ nm, $\lambda = 772$ nm, $\lambda = 1195$ nm and $\lambda = 925$ nm, respectively.

NFR_3, indicating that NFR_3 represents the groove mode. To explain the origin of the quadruple Fano resonances, the distribution of normalized magnetic field intensity ($|H_z|^2$) at the peak of FR_1 ($\lambda = 678$ nm), NFR_1 ($\lambda = 772$ nm), NFR_3 ($\lambda = 1195$ nm) and NFR_4 ($\lambda = 925$ nm) are numerically calculated as displayed in Fig. 6(c)–(f), respectively. According to the field intensity distributions, it is apparent that FR_1, NFR_1 and NFR_3 represent the ring mode, stub mode and groove mode respectively, which corresponds well with the analysis above. And the field intensity at NFR_4 is confined in both the stub and the groove cavity, so it can be called as the stub-groove mode.

Since the quadruple Fano resonances are generated from different modes which are related to the stub and groove cavity in the structure, they can be tuned by changing the parameters of the stub and groove cavity. Herein, we calculated the tuning of the resonant wavelengths on the variable L_1 or L_2, while the other parameters keep fixed. As shown in Fig. 7(a)–(e), when L_1 is fixed at 100 nm and L_2 is altered from 150 nm to 190 nm, NFR_3 makes a red shift from 1183 nm to 1248 nm, and NFR_4 makes a red shift from 908 nm to 977 nm, while FR_1 and NFR_1 keep fixed since they will not be affected by the groove cavity. The tuning of NFR_4 has little effect on NFR_1 but has evident effect on NFR_3, this kind of tuning is called 'semi-independent tuning'. And as shown in Fig. 7(f)–(j), when L_2 is fixed at 160 nm and L_1 is altered from 100 nm to 116 nm, NFR_1 makes a red shift from 772 nm to 794 nm, and NFR_4 makes a red shift from 925 nm to 959 nm, while FR_1 and NFR_3 keep fixed since they will not be affected by the stub cavity. The tuning of NFR_4 has little effect on NFR_3 but has evident effect on NFR_1, this is also 'semi-independent tuning'.

Finally, we further investigate the sensing performance based on the proposed structure, as shown in Fig. 8(a) and (b). The resonant wavelength has a red shift with refractive index increasing from 1 to 1.06. Here, the proposed structure still has good sensitivity, about 1100 nm/RIU for NFR_3 and 950 nm/RIU for NFR_4, which is better compared with those in the references [2], [21], [35]. The FOM curve is shown in Fig. 8(b), and the maximum is as high as FOM $= 2.73 \times 10^4$ at $\lambda = 978$ nm, which is much higher compared with those previous plasmonic sensors reports [4], [18], [26].

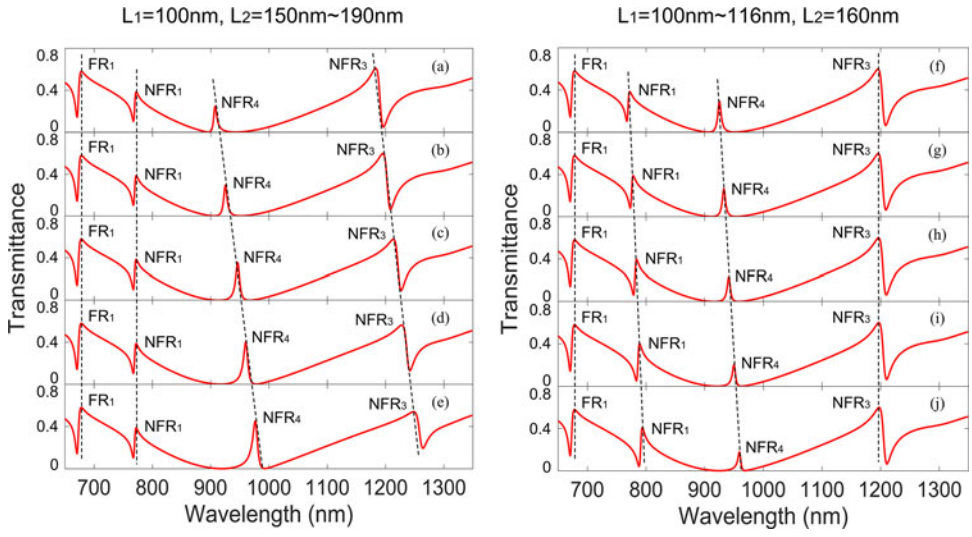

Fig. 7. (a)–(e) Transmission spectra for variable L_2 with $L_1 = 100$ nm. (f)–(j) Transmission spectra for variable L_1 with $L_2 = 160$ nm.

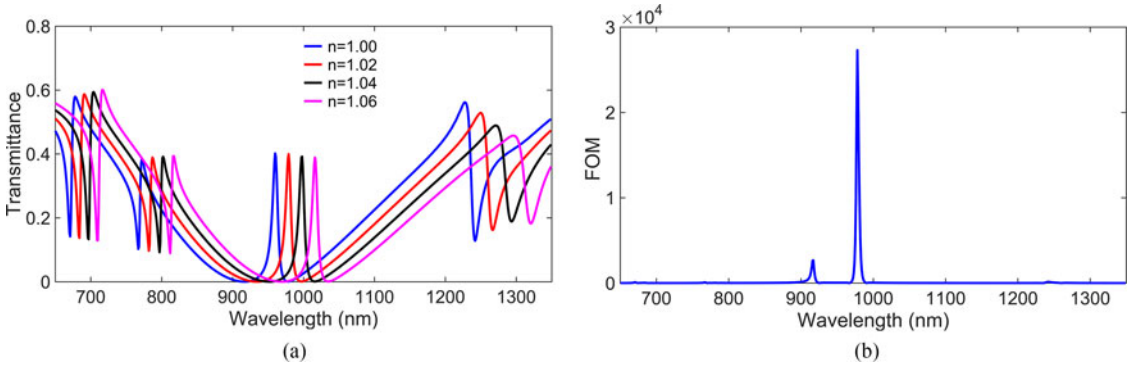

Fig. 8. (a) Transmission spectra for different refractive index. (b) The calculated FOM at different wavelength, the parameters are set as $L_1 = 100$ nm, $L_2 = 180$ nm.

4. Conclusion

In summary, the transmission characteristics of the proposed structure which composed of an MIM waveguide with a disk and a ring cavity are analyzed and investigated using the FDTD method. Simulation results show that the ring cavity supports a discrete state and the disk provides a continuous spectrum, and the interaction between them gives rise to the Fano resonance. In addition, multiple Fano resonances are achieved by adding end-coupled cavities. The multiple Fano resonances originate from different mechanisms and can be tuned semi-independently by changing the parameters of the end-coupled cavities. The proposed structure can work as a highly efficient plasmonic nanosensor with a sensitivity of ~1100 nm/RIU and figure of merit (FOM) of $\sim 2.73 \times 10^4$. The proposed structures may have potential applications in highly integrated photonic circuits and networks, especially for the sensing, slow light and nonlinear devices.

References

[1] A. Miroshnichenko, S. Flach, and Y. Kivshar, "Fano resonances in nanoscale structures," *Rev. Mod. Phys.*, vol. 82, no. 3, pp. 2257–2298, Aug. 2010.

[2] Z. Chen and L. Yu, "Multiple Fano resonances based on different waveguide modes in a symmetry breaking plasmonic system," *IEEE Photon. J.*, vol. 6, no. 6, Nov. 2014, Art. no. 4802208.

[3] J. Chen, Z. Li, X. Zhang, J. Xiao, and Q. Gong, "Submicron bidirectional all-optical plasmonic switches," *Sci. Rep.*, vol. 3, Mar. 2013, Art. no. 1451.
[4] Y. Binfeng, Z. Ruohu, H. Guohua, and C. Yiping, "Ultra sharp Fano resonances induced by coupling between plasmonic stub and circular cavity resonators," *Plasmonics*, vol. 11, no. 4, pp. 1157–1162, Aug. 2016.
[5] F. Nan *et al.*, "Unusual and tunable one-photon nonlinearity in gold-dye plexcitonic Fano systems," *Nano Lett.*, vol. 15, no. 4, pp. 2705–2710, Apr. 2015.
[6] B. Luk'yanchuk *et al.*, "The Fano resonance in plasmonic nanostructures and metamaterials," *Nat. Mater.*, vol. 9, no. 9, pp. 707–715, Sep. 2010.
[7] F. Hao *et al.*, "Symmetry breaking in plasmonic nanocavities: Subradiant LSPR sensing and a tunable Fano resonance," *Nano Lett.*, vol. 8, no. 11, pp. 3983–3988, Nov. 2008.
[8] F. Hao *et al.*, "Tunability of subradiant dipolar and Fano-type plasmon resonances in metallic ring/disk cavities: Implications for nanoscale optical sensing," *ACS Nano*, vol. 3, no. 3, pp. 643–652, Mar. 2009.
[9] A. E. Cetin and H. Altug, "Fano resonant ring/disk plasmonic nanocavities on conducting substrates for advanced biosensing," *ACS Nano*, vol. 6, no. 11, pp. 9989–9995, Nov. 2012.
[10] J. A. Fan *et al.*, "Self-assembled plasmonic nanoparticle clusters," *Science*, vol. 328, no. 5982, pp. 1135–1138, May 2010.
[11] M. Hentschel *et al.*, "Transition from isolated to collective modes in plasmonic oligomers," *Nano Lett.*, vol. 10, no. 7, pp. 2721–2726, Jul. 2010.
[12] K. Bao, N. A. Mirin, and P. Nordlander, "Fano resonances in planar silver nanosphere clusters," *Appl. Phys. A*, vol. 100, no. 2, pp. 333–339, Aug. 2010.
[13] F. Neubrech *et al.*, "Resonant plasmonic and vibrational coupling in a tailored nanoantenna for infrared detection," *Phys. Rev. Lett.*, vol. 101, no. 15, Oct. 2008, Art. no. 157403.
[14] K. C. Woo *et al.*, "universal scaling and Fano resonance in the plasmon coupling between gold nanorods," *ACS Nano*, vol. 5, no. 7, pp. 5976–5986, Jul. 2011.
[15] V. Giannini *et al.*, "Fano resonances in nanoscale plasmonic systems: a parameter-free modeling approach," *Nano Lett.*, vol. 11, no. 7, pp. 2835–2840, Jul. 2011.
[16] Y. Zhu, X. Hu, Y. Huang, H. Yang, and Q. Gong, "Fast and low-power all-optical tunable Fano resonance in plasmonic microstructures," *Adv. Opt. Mater.*, vol. 1, no. 1, pp. 61–67, Jan. 2013.
[17] H. Lu, X. M. Liu, D. Mao, and G. Wang, "Plasmonic nanosensor based on Fano resonance in waveguide-coupled resonators," *Opt. Lett.*, vol. 37, no. 18, pp. 3780–3782, Sep. 2012.
[18] J. Qi *et al.*, "Independently tunable double Fano resonances in asymmetric MIM waveguide structure," *Opt. Exp.*, vol. 22, no. 12, pp. 14688–14695, Jun. 2014.
[19] J. Chen, C. Sun, and Q. Gong, "Fano resonances in a single defect nanocavity coupled with a plasmonic waveguide," *Opt Lett.*, vol. 39, no. 1, pp. 52–55, Jan. 2014.
[20] Z. Chen, X. Song, G. Duan, L. Wang, and L. Yu, "Multiple Fano resonances control in MIM side-coupled cavities systems," *IEEE Photon. J.*, vol. 7, no. 3, Jun. 2015, Art. no. 2701009.
[21] S. Li, Y. Wang, R. Jiao, L. Wang, G. Duan, and L. Yu, "Fano resonances based on multimode and degenerate mode interference in plasmonic resonator system," *Opt. Exp.*, vol. 25, no. 4, pp. 3525–3533, Feb. 2017.
[22] G. Zhan, R. Liang, H. Liang, J. Luo, and R. Zhao, "Asymmetric band-pass plasmonic nanodisk filter with mode inhibition and spectrally splitting capabilities," *Opt. Exp.*, vol. 22, no. 8, pp. 9912–9919, Apr. 2014.
[23] Z. Chen *et al.*, "Symmetry breaking induced mode splitting based on a plasmonic waveguide system," *J. Phys. D, Appl. Phys.*, vol. 49, no. 14, Mar. 2016, Art. no. 145109.
[24] J. Tao, X. G. Huang, X. Lin, Q. Zhang, and X. Jin, "A narrow-band subwavelength plasmonic waveguide filter with asymmetrical multiple-teeth-shaped structure," *Opt. Exp.*, vol. 17, no. 16, pp. 13989–13994, Aug. 2009.
[25] J. Tao, X. G. Huang, X. Lin, J. Chen, Q. Zhang, and X. Jin, "Systematical research on characteristics of double-sided teeth-shaped nanoplasmonic waveguide filters," *J. Opt. Soc. Amer. B*, vol. 27, no. 2, pp. 323–327, Feb. 2010.
[26] S. Li, Y. Zhang, X. Song, Y. Wang, and L. Yu, "Tunable triple Fano resonances based on multimode interference in coupled plasmonic resonator system," *Opt. Exp.*, vol. 24, no. 14, pp. 15351–15361, Jul. 2016.
[27] G. Lai *et al.*, "Double plasmonic nanodisks design for electromagnetically induced transparency and slow light," *Opt. Exp.*, vol. 23, no. 5, pp. 6554–6561, Mar. 2015.
[28] Q. Lu *et al.*, "Plasmon-induced transparency and high-performance slow light in a plasmonic single-mode and two-mode resonators coupled system," *J. Lightw. Technol.*, vol. 35, no. 9, pp. 1710–1717, May 2017.
[29] C. Wu, A. B. Khanikaev, and G. Shvets, "Broadband slow light metamaterial based on a double-continuum Fano resonance," *Phys. Rev. Lett.*, vol. 106, no. 10, Mar. 2011, Art. no. 107403.
[30] A. Artar, A. A. Yanik, and H. Altug, "Directional double Fano resonances in plasmonic hetero-oligomers," *Nano Lett.*, vol. 11, no. 9, pp. 3694–3700, Sep. 2011.
[31] D. Wang, X. Yu, and Q. Yu, "Tuning multiple Fano and plasmon resonances in rectangle grid quasi-3D plasmonic-photonic nanostructures," *Appl. Phys. Lett.*, vol. 103, no. 5, Jul. 2013, Art. no. 053117.
[32] P. B. Johnson and R. W. Christy, "Optical constants of the noble metals," *Phys. Rev. B*, vol. 6, no. 12, pp. 4370–4379, Dec. 1972.
[33] F. Hu, H. Yi, and Z. Zhou, "Wavelength demultiplexing structure based on arrayed plasmonic slot cavities," *Opt. Lett.*, vol. 36, no. 8, pp. 1500–1502, Apr. 2011.
[34] D. Yang, C. Li, C. Wang, Y. Ji, and Q. Quan, "High figure of merit Fano resonance in 2-D defect-free pillar array photonic crystal for refractive index sensing," *IEEE Photon. J.*, vol. 8, no. 6, Dec. 2016, Art. no. 4502414.
[35] N. Liu *et al.*, "Planar metamaterial analogue of electromagnetically induced transparency for plasmonic sensing," *Nano Lett.*, vol. 10, no. 4, pp. 1103–1107, Apr. 2010.